

Edge-Dependent Step-Flow Growth Mechanism in β -Ga₂O₃ (100) Facet at the Atomic Level

Qi Li^{∇,†}, Junlei Zhao^{∇,*‡}, Na Lin,^{*†} Xiufeng Cheng,[†] Xian Zhao,^{†,¶} Zhaojun
Liu,[‡] Zhitai Jia,^{*†,§} and Mengyuan Hua^{*‡}

[†]*State Key Laboratory of Crystal Materials, Institute of Novel Semiconductors, Institute of Crystal materials, Shandong University, Jinan, Shandong, 250100, China*

[‡]*Department of Electronic and Electrical Engineering, Southern University of Science and Technology, Shenzhen, 518055, China*

[¶]*Center for Optics Research and Engineering, Shandong University, Qingdao, Shandong, 266237, China*

[§]*Shandong Research Institute of Industrial Technology, Jinan, Shandong, 250100, China*

E-mail: zhaojl@sustech.edu.cn; linna@sdu.edu.cn; z.jia@sdu.edu.cn; huamy@sustech.edu.cn

Abstract

Homoepitaxial step-flow growth of high-quality β -Ga₂O₃ thin films is essential for the advancement of high-performance Ga₂O₃-based devices. In this work, the step-flow growth mechanism of β -Ga₂O₃ (100) facet is explored by machine-learning molecular dynamics simulations and density functional theory calculations. Our results reveal that Ga adatoms and Ga-O adatom pairs, with their high mobility, are the primary atomic species responsible for efficient surface migration on the (100) facet. The asymmetric monoclinic structure of β -Ga₂O₃ induces a distinct two-stage Ehrlich-Schwoebel barrier for Ga adatoms at the $[00\bar{1}]$ step edge, contributing to the suppression of double-step and hillock formation. Furthermore, a miscut towards $[00\bar{1}]$ does not induce the nucleation of stable twin boundaries, whereas a miscut towards $[001]$ leads

to the spontaneous formation of twin boundaries. This research provides meaningful insights not only for high-quality β -Ga₂O₃ homoepitaxy but also the step-flow growth mechanism of other similar systems.

Keywords

Gallium oxide; Step-flow growth; Machine-learning; Molecular dynamics; Density functional theory

Gallium oxide (Ga₂O₃) has garnered enormous interest from (opto-)electronics community as a promising next-generation ultrawide bandgap semiconductor. Among its polymorphs, the monoclinic β -Ga₂O₃, the most stable phase under ambient conditions, exhibits several remarkable properties, including an ultrawide bandgap ($E_g \simeq 4.9$ eV), a high breakdown electric field ($E_{\text{crit}} \simeq 8$ MV/cm), exceptional chemical and thermal stability (melting point $\simeq 1720$ °C), a large Baliga's figure of merit (BFOM = 3444), and a short ultraviolet cut-off edge of ~ 260 nm¹⁻⁵. Owing to these outstanding material properties, β -Ga₂O₃ possesses great prospects for applications in high-power electronics^{6,7}, solar-blind ultraviolet optoelectronics^{8,9}, and two-dimensional devices¹⁰⁻¹². To fabricate high-performance β -Ga₂O₃-based device, a high-quality epitaxial thin film with a smooth surface and low defect density is essential¹³⁻¹⁵. Particularly, homoepitaxy is significant for minimizing defect density in the β -Ga₂O₃ epitaxial thin film by avoiding lattice mismatch in heteroepitaxy. Recently, the homoepitaxy of β -Ga₂O₃ has been explored using several thin film growth techniques, such as metal-organic vapor phase epitaxy (MOVPE)^{14,16} (also referred to as metal-organic chemical vapor deposition, MOCVD, in the literature^{17,18}), molecular beam epitaxy (MBE)^{15,19}, halide vapor phase epitaxy (HVPE)^{20,21}, and mist chemical vapor deposition (mist-CVD)^{22,23}.

Extensive literature has demonstrated that the facet orientation of β -Ga₂O₃ homoepitaxial substrate can significantly affect the growth kinetics, and hence the quality of the homoepitaxial thin film²⁴⁻²⁹. Among the commonly studied facet orientations, namely, (100), (010), (001), and ($\bar{2}$ 01), the (100) facet is the easiest to prepare and is considered as

the most adequate orientation for the devices requiring smooth surfaces and/or high-quality interfaces. This is because the (100) plane serves as the preferred cleavage plane with the lowest surface energy in $\beta\text{-Ga}_2\text{O}_3$ ^{30,31}. However, the main challenge associated with homoepitaxy on the (100) $\beta\text{-Ga}_2\text{O}_3$ substrate is the possibility of forming twin boundary with high density due to Ga-sublattice double positioning^{32,33}. As a remedy, it has been demonstrated that by introducing miscuts towards $[00\bar{1}]$ on substrates oriented to (100) plane, the epitaxial growth of $\beta\text{-Ga}_2\text{O}_3$ can achieve stable step-flow growth and obtain epitaxial thin films with excellent crystal quality^{14,16,32,34-36}.

The step-flow growth mode is an epitaxial process in which deposited adatoms migrate to step edges between adjacent atomic layers on a surface before nucleating on terraces. This mechanism enables smooth, layer-by-layer growth while preventing the formation of hillocks on terraces, ultimately resulting in smooth film surfaces with high crystalline quality^{37,38}. Therefore, exploring the atomic mechanisms underlying the step-flow growth and achieving morphology control in $\beta\text{-Ga}_2\text{O}_3$ homoepitaxy is of great significance from both fundamental and application perspectives. A particularly important factor in step-flow epitaxial growth is the Ehrlich-Schwoebel (ES) barrier (denoted as E_{ES}), which refers to the additional energy barrier for adatoms to overcome when diffusing across a surface step edge³⁹⁻⁴¹. A large E_{ES} can lead to step-edge meandering and terrace morphology alteration, potentially destabilizing the step-flow growth⁴²⁻⁴⁴.

In recent studies, numerical models³² have been developed and experimentally validated to describe the morphology control of (100) $\beta\text{-Ga}_2\text{O}_3$ films grown by MOVPE^{14,16}. However, the exploration of the complex kinetic and thermodynamic evolution of the step-flow growth processes at the atomic scale is still lacking. Furthermore, the migration barrier and path of adatoms on the surface of $\beta\text{-Ga}_2\text{O}_3$ substrates must be clarified to determine the E_{ES} and explain the essential mechanism of the step-flow growth of $\beta\text{-Ga}_2\text{O}_3$. In this work, the mechanism of the step-flow growth of $\beta\text{-Ga}_2\text{O}_3$ on the (100) substrates with different miscuts was demonstrated at the atomic resolution. Specifically, the minimum energy paths

(MEPs) and minimum energy barriers (MEBs) of adatoms on the (1 0 0) β -Ga₂O₃ substrates with and without miscuts were revealed using nudged elastic band (NEB) method. The complex dynamic evolution and accurate energetics were explored using machine-learning molecular dynamics (ML-MD) simulations, and density functional theory (DFT) calculations. Furthermore, we emphasized that the inherently asymmetric atomic configurations at the miscut $[0 0 \bar{1}]$ and $[0 0 1]$ step edges result in distinct kinetic and thermodynamic evolution of Ga and O atomic migrations. Additionally, the differences in nucleation energies of twin boundaries (TBs) at these two different miscut step edges provide a compelling explanation for the variations in epitaxy quality observed in recent experimental studies^{14,16,34}.

Before investigating atomic migrations at the miscut step edges, we first examine the migration behavior of Ga/O adatoms and Ga-O adatom pair on the flat (1 0 0) surface of β -Ga₂O₃, as predicted by the ML model, as illustrated in Figure 1. We conducted a comprehensive search of atomic migration paths (detailed in Supporting Information Note 1, Figures S1 and S2, and Table S1), closely examining all the possible direct hopping/exchange migration paths. The MEPs in the $[0 0 1]/[0 0 \bar{1}]$ directions on the (1 0 0) surface involve direct hopping for the Ga/O adatoms (Figure 1a and 1b) and Ga exchange for the Ga-O adatom pair (Figure 1c). The corresponding MEBs for Ga adatom, O adatom, and Ga-O adatom pair were found to be 1.15 eV, 1.53 eV, and 0.56 eV, respectively. We also validated these ML-predicted MEPs and MEBs through DFT calculations (Supporting Information Note 1, Figure S4), which exhibited the same trends with reasonable deviation. Based on the ML and DFT results, the mobility of Ga adatom is consistently higher than that of O adatom. The Ga-O adatom pair can enhance the migration of surface adatoms, by facilitating the exchange migration path. These results provide important references for the subsequent exploration of atomic migration on the (1 0 0) surface with different miscut step edges.

We further investigated the MEPs and MEBs of Ga/O adatom migration on the β -Ga₂O₃ (1 0 0) surface with two miscut step edges, as shown in Figure 2. The left step is a $[0 0 \bar{1}]$ step with a $(\bar{2} 0 1)$ step-edge facet, and the right step is a $[0 0 1]$ step with a $(0 0 1)$ step-edge facet.

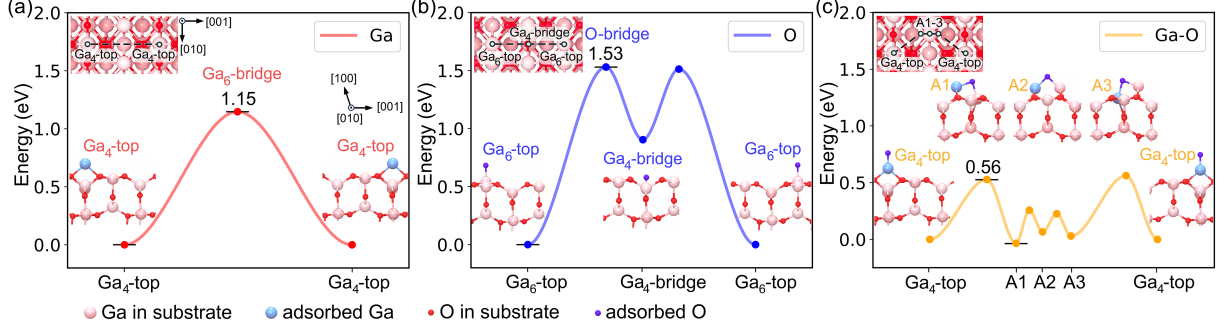


Figure 1: MEBs for (a) a Ga adatom (big lightblue sphere), (b) an O adatom (small purple sphere), and (c) a Ga-O adatom pair on the (100) surface of β -Ga₂O₃. Substrate Ga and O atoms are shown in pink and red, respectively. Insets at the top-left corners of the three panels provide the top views of the corresponding MEPs. The curves represent the fitted MEBs, with each valley point corresponding to the adjacent structure. Ga₄ and Ga₆ denote the four-coordinated and six-coordinated Ga substrate sites, respectively.

The atomic migration paths at the step edges on the both sides were searched systematically (see Supporting Information, Note 2, Figure S5, and Tables S2 and S3). The MEPs on the terrace are the same as those on the flat (100) surface (Figure 1), whereas the MEBs exhibit marginal increases (1.29 eV *vs.* 1.15 eV for Ga and 1.65 eV *vs.* 1.53 eV for O), owing to the compressive strain effect of the stepped terrace.

Importantly, the most striking observation is the distinct single- and two-stage ES barriers of Ga adatom, rooted from the asymmetric monoclinic lattice of β -Ga₂O₃. As shown in Figure 2a, the overall MEB for migrating downward the $[00\bar{1}]$ step edge (Ga_V → Ga_{IV} → Ga_{III}) is $E_{S(201)} = 1.44$ eV. In comparison to the MEB climbing downward the $[001]$ step edge (Ga_{VI} → Ga_{VII}, $E_{S(001)} = 1.52$ eV), the energy difference in the ES barriers is not significant (0.15 eV *vs.* 0.23 eV). However, a two-stage MEP is revealed for migrating downward the $[00\bar{1}]$ step edge, where the Ga_{IV} site serves as a metastable shallow valley with an effective downhill barrier of $E'_{S(201)} = 0.54$ eV. In addition to the overall smaller $[00\bar{1}]$ ES barrier (0.15 eV), this intermediate Ga_{IV} site (similar to an intermediate state in catalysis) can significantly promote the downhill migration of Ga adatom at the $[00\bar{1}]$ step edge, thereby suppressing the formation of double-steps and hillocks on the terrace in the $[00\bar{1}]$ miscut direction.

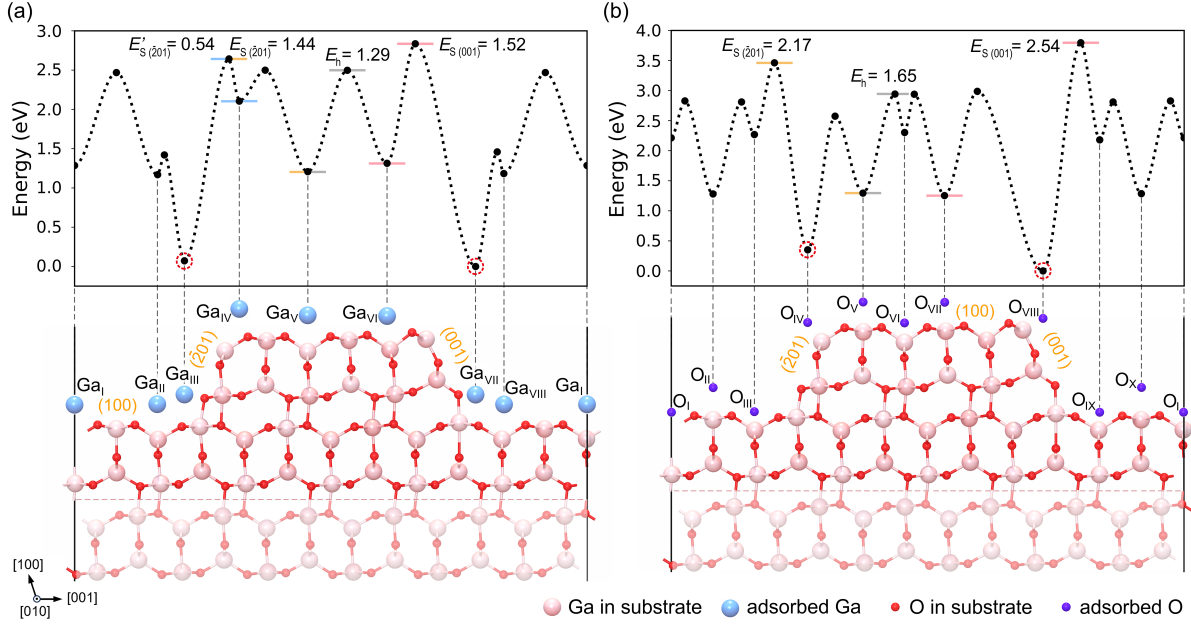


Figure 2: The overall MEBs of (a) Ga and (b) O adatoms on the (100) surface with two miscut step edges. The black dashed curves in the upper panels represent the fitted MEBs. The valley points of the curves correspond to metastable adsorption sites which are represented as blue or purple spheres for adsorbed Ga or O, respectively. The lowest energy sites at the two step edges are marked with red dashed circles. The zero energy is leveled to the global energy minima of the two curves.

Additionally, the energies of Ga adatoms at the step-edge-bottom sites (Ga_{III} and Ga_{VII}) are much lower, compared to the energies at the step-edge-top sites (Ga_{IV} and Ga_{VI}). These energy differences lead to a strong downhill migration trend for Ga adatoms at the step edge. These results have been validated by DFT calculations, which can be found in Supporting Information, Note 2, Figures S5 and S7. For comparison, we also calculated the MEBs of Ga adatoms on a step with the $(\bar{2}01)$ terrace and (100) step-edge surface (see Supporting Information, Note 2, Figure S8), showing a much higher MEBs and ES barriers. On the other hand, the MEBs of O adatom migration on both terrace and step edges are higher than those of Ga adatom, as shown in Figure 2b. Notably, unlike the stable Ga sites, the most stable sites near the step edges for O adatoms are the step-edge-top sites, which is expected for anions, as the step-edge-bottom sites are screened by the O anions carrying the same type of charge.

However, although the NEB calculations for the migration of Ga and O adatoms provide clear evidence on the edge-dependent step-flow growth mechanism, arising from the asymmetry of $\beta\text{-Ga}_2\text{O}_3$ lattice, the manybody (such as Ga-O adatom pair and more) migration is too complicated to be effectively described by MEPs and MEBs. Therefore, we further conducted ML-MD simulations to elucidate the dynamic migration process for Ga/O adatoms, and Ga-O adatom pairs on a large-sized $\beta\text{-Ga}_2\text{O}_3$ (100) facet with a miscut $[00\bar{1}]$ step edge.

As shown in Figure 3a, in the random adatom migration simulations, Ga/O adatoms and Ga-O adatom pairs were deposited 10 times at each of the 11 different deposition sites, marked by yellow arrows. The final positions of the adatoms (and pairs) were tracked and counted after annealing for 1500 ps at 1200 K (see Supporting Information, Note 3 for details). The Ga-O adatom pairs tend to migrate quickly to the more stable vicinal sites of the step edges (Sites 1 and 11), exhibiting the highest mobility among the three species tested. Ga adatoms show the second-highest migration mobility, as indicated by the higher count at Site 1, while the distribution of the final O adatom sites remains relatively uniform, with no significant atomic migration. These statistics are in good agreement with the MEBs shown in Figure 1. Notably, the relatively high mobility of Ga adatom and Ga-O adatom pair leads to an essential assumption for the subsequent deposition ML-MD simulations, which consider terrace widths of a few nanometers and time spans of a few nanoseconds: Within a reasonable MD simulation time, the adatoms can migrate to the step-edge region across the full width of the terrace. Consequently, the epitaxial step-flow growth is insensitive to the initial deposition sites of adatoms, as low-mobility O adatoms can be mobilized by forming Ga-O adatom pairs upon encountering Ga adatoms.

Based on this observation and discussion, we further simulated the dynamic processes of epitaxial growth at the $\beta\text{-Ga}_2\text{O}_3$ (100)- $[00\bar{1}]$ step edges, as shown in the snapshots in Figure 3b-g (More details in Supporting Information, Note 3, Figures S9 and S10, and Movies S1 and S2). The deposited adatoms near the step edge quickly bind to the edge-bottom site, and then grow epitaxially, completing the atomic rings in the sequence indicated

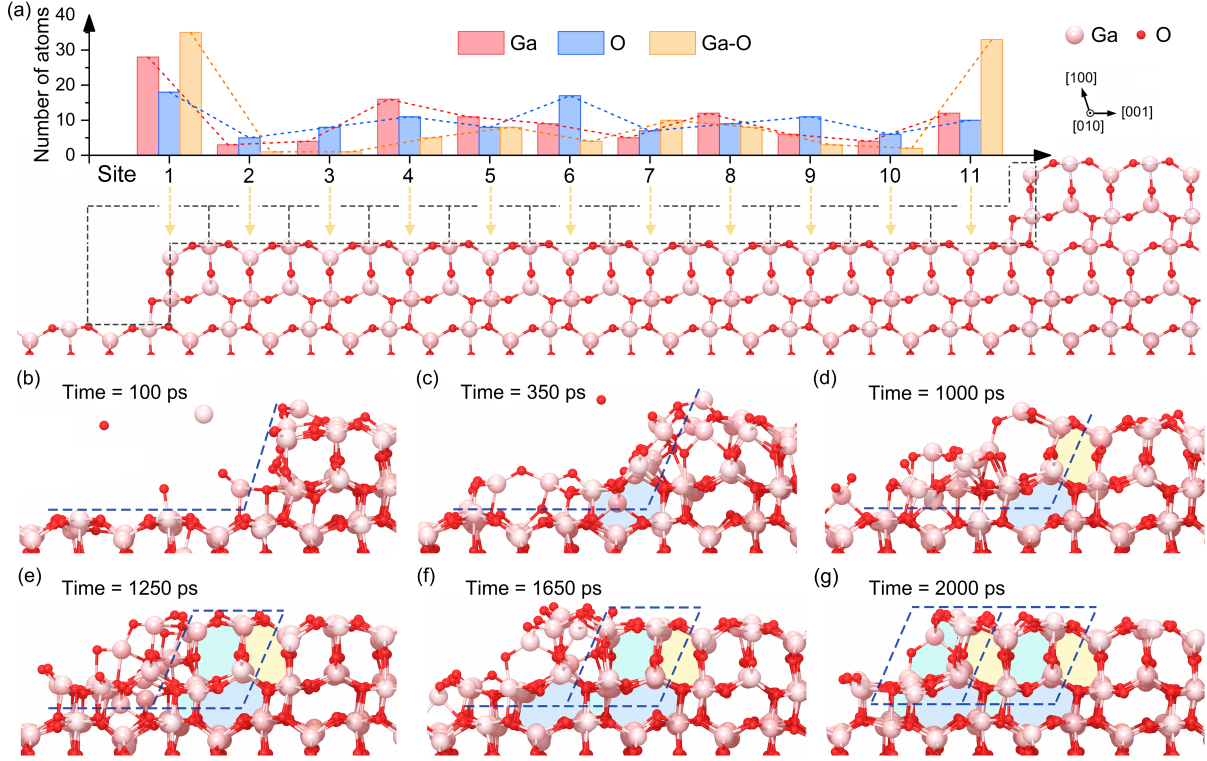


Figure 3: The ML-MD simulations of atomic migration and epitaxial step-flow growth on the (100) substrate with a $[00\bar{1}]$ miscut step. (a) The number of Ga/O adatoms and Ga-O adatom pairs migrating to different site regions after annealing for 1500 ps at 1200 K. Each type of adatom (and pair) is deposited 10 times at all the 11 sites marked by the yellow arrows. (b-g) The snapshots of step-flow growth of β -Ga₂O₃ on the (100)- $[00\bar{1}]$ step at 1200 K. The dashed lines in panels (b-g) distinguish the initial substrate. The colored shadows indicate the atomic rings characteristic of β -Ga₂O₃. A completed periodic unit of epitaxial ($\bar{2}01$) step edge is highlighted by a blue dashed parallelogram. See Supporting Information, Movie S1, for the full process.

by the “blue \rightarrow yellow \rightarrow cyan \rightarrow blue” shadows in Figure 3b-g. The epitaxial layer initially grows a half-layer extending the step edge (blue shadow in Figure 3c) before forming the upper half-layer near the step-edge surface (yellow and cyan shadows in Figure 3d and 3e). Once one period of the epitaxial ($\bar{2}01$) step edge is completed, a second ($\bar{2}01$) step-edge unit can be formed, repeating the step-flow growth process in the $[00\bar{1}]$ direction (depicted by the additional blue, yellow, and cyan shadows in Figure 3f and 3g).

Meanwhile, the step-flow growth process at the (100)- $[00\bar{1}]$ step edge can be investigated by ML-MD simulation, as shown in Supporting Information, Note 3, Figure S10. Notably,

in contrast to the perfect step-flow growth observed at the $[00\bar{1}]$ step edge, the nucleation of TBs was observed in the simulations at the $[001]$ step edge. These findings are consistent with the previous experimental observations^{32,34}, which reported significant lower quality of β -Ga₂O₃ epitaxial films grown on the (100)- $[001]$ step substrates compared to those grown on the (100)- $[00\bar{1}]$ step substrates, primarily due to the high density of TBs. Our ML-MD simulations suggest that these TBs in the epitaxial films may originate from the deposited atoms near the $[001]$ step edge or even from the structural transformations of the step edge itself.

To explain why it is easier to form TBs on the $[001]$ step compared to the $[00\bar{1}]$ step, we conducted further static energy calculations for TB nucleation using the ML model. DFT calculations were also employed to ensure higher accuracy and provide cross-validation. As shown in Figure 4, we constructed the TBs on both the $[00\bar{1}]$ and $[001]$ step edges, considering two different types of atomic structures of TBs at each step edge. The two different TB structures for each step edge are distinguished by the different positions of TB- $(\bar{1}02)$ (Ga₄ and Ga₆ sites), as each twin at the step edge is composed of TB- $(\bar{1}02)$ and TB- (100) . The relaxed structures of these steps with TBs are shown in Supporting Information, Note 4, Figure S11. The energy differences between the TB and perfect step configurations are shown in Figure 4b. For the $[00\bar{1}]$ step, both TB structures shown in Figure 4a are energetically unstable and spontaneously relax back into the perfect step after structure relaxation. On the contrary, for the $[001]$ step, both TB structures shown in Figure 4c are, rather surprisingly, energetically favorable, with energy differences of -0.47 eV/Å and -0.39 eV/Å compared to the perfect step. Therefore, while TBs are energetically unfavorable to form on the $[00\bar{1}]$ step edge, they are energetically favorable and easy to form on the $[001]$ step edge. Our results provide a direct explanation for the phenomena observed in previous experiments^{32,34} as well as in our ML-MD simulations.

Therefore, to achieve the high quality step-flow growth in the homoepitaxy of β -Ga₂O₃, the selection of the orientation of substrates and the directions of miscuts are essential, which

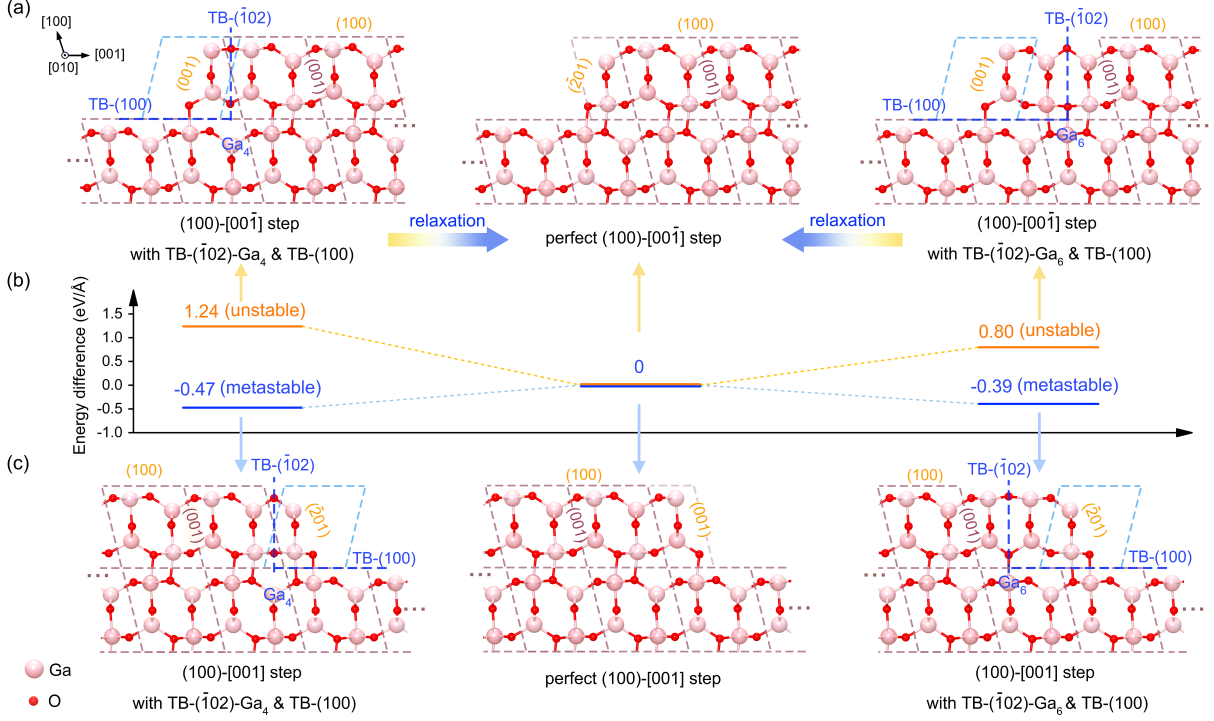


Figure 4: The TB structures of β - Ga_2O_3 at (a) (100) - $[00\bar{1}]$ step edges and (c) (100) - $[001]$ step edges, and (b) the energy differences between these TB structures and the perfect step. The TBs are represented by dark blue dashed lines. The perfect lattice and twins lattice are marked with pink and light blue dashed parallelogram boxes, respectively.

determines the terrace facet and step edge. It is important that atoms can migrate to the step-edge site efficiently, which requires that the migration energy of atoms on the terrace surface is low and the energy of atoms at the step-edge site is significantly lower than that of other sites, as shown in Figure 2 and Figure 3a. Furthermore, both the terrace and step edge surfaces should have good thermal stability to maintain the regular step surface. Notably, even when the above requirements are satisfied, an improper miscut direction can promote the formation of TBs. For instance, the (100) - $[001]$ step edges illustrated in Figure 4 can facilitate TBs formation. In contrast, the atomic structures of the (100) - $[00\bar{1}]$ step edges could effectively prevent the occurrence of TBs.

In this work, we investigated the atomic mechanisms of the step-flow growth on β - Ga_2O_3 (100) facet using ML-MD and DFT methods. Ga adatom and Ga-O adatom pair are the primary atomic species responsible for efficient atomic migration on the (100) surface, both

with and without a miscut, owing to their relatively low MEBs. The intrinsic lattice asymmetry of $\beta\text{-Ga}_2\text{O}_3$ leads to a distinct two-stage ES barrier of Ga adatoms at the $[00\bar{1}]$ step edge, favoring downhill migration towards the stable step-edge-bottom site. The periodic step-flow growth processes on the $(100)\text{-}[00\bar{1}]$ and $(100)\text{-}[001]$ step edges are revealed through ML-MD simulations at atomic resolution. Furthermore, the TB nucleation structures at the $(100)\text{-}[001]$ step edge are proved to be energetically more favorable than the perfect step, while the TB structures on the $(100)\text{-}[00\bar{1}]$ step edges are unstable. Our study clarifies the mechanisms of the step-flow growth on $\beta\text{-Ga}_2\text{O}_3$ (100) substrates, providing an atom-level theoretical basis for the selection and processing of substrates to achieve high-quality $\beta\text{-Ga}_2\text{O}_3$ epitaxial thin films.

Methodology

The ML-MD calculations in this work are performed using the Large-scale Atomic/Molecular Massively Parallel Simulator (LAMMPS) code⁴⁵. The ML interatomic potential was recently developed in our previous work⁴⁶ makes the large-scale MD simulations of Ga_2O_3 homoepitaxy feasible²⁹ and high-energy collision cascade. The atomic migration MEBs were calculated by the climbing-image nudged elastic band (CI-NEB) method with improved tangent estimation^{47,48}, converging the forces to within 1×10^{-3} eV/Å and energies to within 1×10^{-6} eV. These NEB calculations were performed using 9 images between the initial and final structures. For MD simulations of the $\beta\text{-Ga}_2\text{O}_3$ homoepitaxy and the migration of Ga/O atoms or Ga-O atomic pair on the step surface, the temperature were set as 1200 K. All the MD simulation cells consist of three groups of atoms depending on the initial positions: (i) the atoms in the fixed layer are fixed to avoid movement of the entire cell due to the momentum introduced by the incoming deposited atoms; (ii) the atoms in the thermal layer are controlled by Nosé-Hoover thermostat^{49,50}; and (iii) the atoms in the surface layer, epilayer, and deposition zone are allowed to move freely following Newton’s law. More details

on ML-MD calculations can be found in the Supporting Information, Note 3.

All of our DFT calculations are performed using Vienna Ab-initio Simulation Package (VASP) code⁵¹ with the projected augmented-wave (PAW) method⁵², employing 13 ($3d^{10}4s^24p^1$) and 6 ($2s^22p^4$) valence electrons for Ga and O atoms, respectively. The generalized gradient approximation (GGA) with Perdew-Burke-Ernzerhof (PBE)⁵³ functional is used for xc -correlation. The kinetic energy cutoff of the plane-wave is set to 520 eV. For structural optimization, the energy convergence criterion was 1×10^{-5} eV, and the force convergence criterion was 1×10^{-2} eV/Å. Gaussian approximated smearing with a width of 0.01 eV was used. The MEBs of atomic migration were calculated using the CI-NEB method by VASP-vtst^{47,48}, converging the forces to within 5×10^{-2} eV/Å. More details on DFT calculations can be found in the Supporting Information, Notes 1 and 4. The OVITO are used for the purpose of analyzing and visualizing the atomic configuration⁵⁴.

The energy differences (E_{diff}) between the TB structures and perfect step are calculated by the following formula:

$$E_{\text{diff}} = \frac{1}{L}(E_{\text{TB}} - E_{\text{perf}}), \quad (1)$$

where the E_{TB} and E_{perf} are the energy of the TB structures and the energy of the perfect step structure, respectively; L is the length of cells in the $[010]$ direction, which is 6.17 Å in our work.

References

- (1) Vllora, E. G.; Shimamura, K.; Yoshikawa, Y.; Ujiie, T.; Aoki, K. Electrical conductivity and carrier concentration control in β -Ga₂O₃ by Si doping. *Appl. Phys. Lett.* **2008**, *92*, 202120, DOI: 10.1063/1.2919728.
- (2) Onuma, T.; Saito, S.; Sasaki, K.; Masui, T.; Yamaguchi, T.; Honda, T.; Higashiwaki, M. Valence band ordering in β -Ga₂O₃ studied by polarized transmittance and reflectance spectroscopy. *Jpn. J. Appl. Phys.* **2015**, *54*, 112601, DOI: 10.7567/JJAP.54.112601.

- (3) Pearton, S. J.; Yang, J.; Cary, P. H.; Ren, F.; Kim, J. H.; Tadjer, M. J.; Mastro, M. A. A review of Ga₂O₃ materials, processing, and devices. *Appl. Phys. Rev.* **2018**, *5*, 011301, DOI: 10.1063/1.5006941.
- (4) Arora, K.; Goel, N.; Kumar, M.; Kumar, M. Ultrahigh performance of self-powered β -Ga₂O₃ Thin Film solar-blind photodetector grown on cost-effective Si substrate using high-temperature seed layer. *ACS Photonics* **2018**, *5*, 2391, DOI: 10.1021/acsp Photonics.8b00174.
- (5) Kaur, D.; Kumar, M. A strategic review on gallium oxide based deep-ultraviolet photodetectors: recent progress and future prospects. *Adv. Opt. Mater.* **2021**, *9*, 2002160, DOI: 10.1002/adom.202002160.
- (6) Sasaki, K.; Higashiwaki, M.; Kuramata, A.; Masui, T.; Yamakoshi, S. MBE grown Ga₂O₃ and its power device applications. *J. Cryst. Growth* **2013**, *378*, 591–595, DOI: 10.1016/j.jcrysgro.2013.02.015.
- (7) Zhang, J.; Dong, P.; Dang, K.; Zhang, Y.; Yan, Q.; Xiang, H.; Su, J.; Liu, Z.; Si, M.; Gao, J.; Kong, M.; Zhou, H.; Hao, Y. Ultra-wide bandgap semiconductor Ga₂O₃ power diodes. *Nat. Commun.* **2022**, *13*, 3900, DOI: 10.1038/s41467-022-31664-y.
- (8) Higashiwaki, M.; Jessen, G. H. Guest Editorial: The dawn of gallium oxide microelectronics. *Appl. Phys. Lett.* **2018**, *112*, 060401, DOI: 10.1063/1.5017845.
- (9) Wang, Y.; Li, H.; Cao, J.; Shen, J.; Zhang, Q.; Yang, Y.; Dong, Z.; Zhou, T.; Zhang, Y.; Tang, W.; Wu, Z. Ultrahigh gain solar blind avalanche photodetector using an amorphous Ga₂O₃-based heterojunction. *ACS Nano* **2021**, *15*, 16654, DOI: 10.1021/acsnano.1c06567.
- (10) Aljarb, A. et al. Ledge-directed epitaxy of continuously self-aligned single-crystalline nanoribbons of transition metal dichalcogenides. *Nat. Mater.* **2020**, *19*, 1300–1306, DOI: 10.1038/s41563-020-0795-4.

- (11) Zhao, J.; Huang, X.; Yin, Y.; Liao, Y.; Mo, H.; Qian, Q.; Guo, Y.; Chen, X.; Zhang, Z.; Hua, M. Two-dimensional gallium oxide monolayer for gas-sensing application. *J. Phys. Chem. Lett.* **2021**, *12*, 5813–5820, DOI: 10.1021/acs.jpcllett.1c01393.
- (12) Yi, K. et al. Integration of high- κ native oxides of gallium for two-dimensional transistors. *Nat. Electron.* **2024**, *7*, 1126–1136, DOI: 10.1038/s41928-024-01286-x.
- (13) Vaidya, A.; Sarker, J.; Zhang, Y.; Lubecki, L.; Wallace, J.; Poplawsky, J. D.; Sasaki, K.; Kuramata, A.; Goyal, A.; Gardella, J. A.; Mazumder, B.; Singiseti, U. Structural, band and electrical characterization of β -(Al_{0.19}Ga_{0.81})₂O₃ films grown by molecular beam epitaxy on Sn doped β -Ga₂O₃ substrate. *J. Appl. Phys.* **2019**, *126*, 095702, DOI: 10.1063/1.5113509.
- (14) Bin Anooz, S.; Grüneberg, R.; Wouters, C.; Schewski, R.; Albrecht, M.; Fiedler, A.; Irmscher, K.; Galazka, Z.; Miller, W.; Wagner, G.; Schwarzkopf, J.; Popp, A. Step flow growth of β -Ga₂O₃ thin films on vicinal (100) β -Ga₂O₃ substrates grown by MOVPE. *Appl. Phys. Lett.* **2020**, *116*, 182106, DOI: 10.1063/5.0005403.
- (15) Mauze, A.; Zhang, Y.; Itoh, T.; Wu, F.; Speck, J. S. Metal oxide catalyzed epitaxy (MO-CATAXY) of β -Ga₂O₃ films in various orientations grown by plasma-assisted molecular beam epitaxy. *APL Mater.* **2020**, *8*, 021104, DOI: 10.1063/1.5135930.
- (16) Chou, T.-S.; Rehm, J.; Bin Anooz, S.; Ernst, O.; Akhtar, A.; Galazka, Z.; Miller, W.; Albrecht, M.; Seyidov, P.; Fiedler, A.; Popp, A. Exploring miscut angle influence on (100) β -Ga₂O₃ homoepitaxial films growth: Comparing MOVPE growth with MBE approaches. *J. Appl. Phys.* **2023**, *134*, 195301, DOI: 10.1063/5.0170463.
- (17) Zhang, T.; Cheng, Q.; Li, Y.; Hu, Z.; Ma, J.; Yao, Y.; Zhang, Y.; Zuo, Y.; Feng, Q.; Zhang, Y.; Zhou, H.; Ning, J.; Zhang, C.; Zhang, J.; Hao, Y. Investigation of the surface optimization of β -Ga₂O₃ films assisted deposition by pulsed MOCVD. *Scr. Mater.* **2022**, *213*, 114623, DOI: 10.1016/j.scriptamat.2022.114623.

- (18) Meng, L.; Yu, D.; Huang, H.-L.; Chae, C.; Hwang, J.; Zhao, H. MOCVD Growth of β -Ga₂O₃ on (001) Ga₂O₃ Substrates. *Cryst. Growth. Des.* **2024**, *24*, 3737, DOI: 10.1021/acs.cgd.4c00060.
- (19) Kuang, S.; Yang, Z.; Zhang, Z.; Sheng, Z.; Wei, S.; Chen, Y.; Xu, W.; Yang, Y.; Chen, D.; Qi, H.; Zhang, K. H. Transport and electronic structure properties of MBE grown Sn doped Ga₂O₃ homo-epitaxial films. *Mater. Today Phys.* **2024**, *48*, 101555, DOI: 10.1016/j.mtphys.2024.101555.
- (20) Leach, J. H.; Uduary, K.; Rumsey, J.; Dodson, G.; Splawn, H.; Evans, K. R. Halide vapor phase epitaxial growth of β -Ga₂O₃ and α -Ga₂O₃ films. *APL Mater.* **2018**, *7*, 022504, DOI: 10.1063/1.5055680.
- (21) Sdoeung, S.; Sasaki, K.; Masuya, S.; Kawasaki, K.; Hirabayashi, J.; Kuramata, A.; Kasu, M. Stacking faults: Origin of leakage current in halide vapor phase epitaxial (001) β -Ga₂O₃ Schottky barrier diodes. *Appl. Phys. Lett.* **2021**, *118*, 172106, DOI: 10.1063/5.0049761.
- (22) Isomura, N.; Nagaoka, T.; Watanabe, Y.; Kutsuki, K.; Nishinaka, H.; Yoshimoto, M. Determination of Zn-containing sites in β -Ga₂O₃ film grown through mist chemical vapor deposition via X-ray absorption spectroscopy. *Jpn. J. Appl. Phys.* **2020**, *59*, 070909, DOI: 10.35848/1347-4065/ab9fdf.
- (23) Nishinaka, H.; Nagaoka, T.; Kajita, Y.; Yoshimoto, M. Rapid homoepitaxial growth of (010) β -Ga₂O₃ thin films via mist chemical vapor deposition. *Mater. Sci. Semicond. Process.* **2021**, *128*, 105732, DOI: 10.1016/j.mssp.2021.105732.
- (24) Feng, Z.; Anhar Uddin Bhuiyan, A. F. M.; Karim, M. R.; Zhao, H. MOCVD homoepitaxy of Si-doped (010) β -Ga₂O₃ thin films with superior transport properties. *Appl. Phys. Lett.* **2019**, *114*, 250601, DOI: 10.1063/1.5109678.

- (25) Mazzolini, P.; Falkenstein, A.; Wouters, C.; Schewski, R.; Markurt, T.; Galazka, Z.; Martin, M.; Albrecht, M.; Bierwagen, O. Substrate-orientation dependence of β -Ga₂O₃ (100), (010), (001), and (-201) homoepitaxy by indium-mediated metal-exchange catalyzed molecular beam epitaxy (MEXCAT-MBE). *APL Mater.* **2020**, *8*, 011107, DOI: 10.1063/1.5135772.
- (26) Ngo, T. S.; Le, D. D.; Lee, J.; Hong, S.-K.; Ha, J.-S.; Lee, W.-S.; Moon, Y.-B. Investigation of defect structure in homoepitaxial (-201) β -Ga₂O₃ layers prepared by plasma-assisted molecular beam epitaxy. *J. Alloys Compd.* **2020**, *834*, 155027, DOI: 10.1016/j.jallcom.2020.155027.
- (27) Meng, L.; Bhuiyan, A. F. M. A. U.; Feng, Z.; Huang, H.-L.; Hwang, J.; Zhao, H. Metalorganic chemical vapor deposition of (100) β -Ga₂O₃ on on-axis Ga₂O₃ substrates. *J. Vac. Sci. Technol., A* **2022**, *40*, 062706, DOI: 10.1116/6.0002179.
- (28) Goto, K.; Murakami, H.; Kuramata, A.; Yamakoshi, S.; Higashiwaki, M.; Kumagai, Y. Effect of substrate orientation on homoepitaxial growth of β -Ga₂O₃ by halide vapor phase epitaxy. *Appl. Phys. Lett.* **2022**, *120*, 102102, DOI: 10.1063/5.0087609.
- (29) Zhang, J.; Zhao, J.; Chen, J.; Hua, M. Orientation-dependent atomic-scale mechanism and defect evolution in β -Ga₂O₃ thin film epitaxial growth. *Appl. Phys. Lett.* **2024**, *124*, 022102, DOI: 10.1063/5.0177093.
- (30) Mu, S.; Wang, M.; Peelaers, H.; Van de Walle, C. G. First-principles surface energies for monoclinic Ga₂O₃ and Al₂O₃ and consequences for cracking of (Al_xGa_{1-x})₂O₃. *APL Mater.* **2020**, *8*, 091105, DOI: 10.1063/5.0019915.
- (31) Chou, T.-S.; Seyidov, P.; Bin Anooz, S.; Grüneberg, R.; Tran, T. T. V.; Irmischer, K.; Albrecht, M.; Galazka, Z.; Schwarzkopf, J.; Popp, A. Fast homoepitaxial growth of (100) β -Ga₂O₃ thin films via MOVPE. *AIP Adv.* **2021**, *11*, 115323, DOI: 10.1063/5.0069243.

- (32) Schewski, R.; Baldini, M.; Irmscher, K.; Fiedler, A.; Markurt, T.; Neuschulz, B.; Remmele, T.; Schulz, T.; Wagner, G.; Galazka, Z.; Albrecht, M. Evolution of planar defects during homoepitaxial growth of β -Ga₂O₃ layers on (100) substrates-A quantitative model. *J. Appl. Phys.* **2016**, *120*, 225308, DOI: 10.1063/1.4971957.
- (33) Li, Q.; Guan, X.; Zhong, Y.; Jia, Z.; Li, Y.; Lin, N. Structures, influences, and formation mechanism of planar defects on (100), (001) and (-201) planes in β -Ga₂O₃ crystals. *Phys. Chem. Chem. Phys.* **2024**, *26*, 12564–12572, DOI: 10.1039/D3CP04305C.
- (34) Schewski, R. et al. Step-flow growth in homoepitaxy of β -Ga₂O₃ (100)-The influence of the miscut direction and faceting. *APL Mater.* **2018**, *7*, 022515, DOI: 10.1063/1.5054943.
- (35) Mazzolini, P.; Falkenstein, A.; Galazka, Z.; Martin, M.; Bierwagen, O. Offcut-related step-flow and growth rate enhancement during (100) β -Ga₂O₃ homoepitaxy by metal-exchange catalyzed molecular beam epitaxy (MEXCAT-MBE). *Appl. Phys. Lett.* **2020**, *117*, 222105, DOI: 10.1063/5.0031300.
- (36) Chou, T.-S.; Rehm, J.; Bin Anooz, S.; Wouters, C.; Ernst, O.; Akhtar, A.; Galazka, Z.; Albrecht, M.; Fiedler, A.; Popp, A. Impurity-induced step pinning and recovery in MOVPE-grown (100) β -Ga₂O₃ film. *Appl. Phys. Lett.* **2025**, *126*, 022101, DOI: 10.1063/5.0242301.
- (37) Matsunami, H.; Kimoto, T. Step-controlled epitaxial growth of SiC: High quality homoepitaxy. *Mater. Sci. Eng. R Rep.* **1997**, *20*, 125–166, DOI: 10.1016/S0927-796X(97)00005-3, R20.
- (38) Hong, W.; Lee, H. N.; Yoon, M.; Christen, H. M.; Lowndes, D. H.; Suo, Z.; Zhang, Z. Persistent step-glow growth of strained films on vicinal substrates. *Phys. Rev. Lett.* **2005**, *95*, 095501, DOI: 10.1103/PhysRevLett.95.095501.

- (39) Schwoebel, R. L.; Shipsey, E. J. Step Motion on Crystal Surfaces. *J. Appl. Phys.* **1966**, *37*, 3682–3686, DOI: 10.1063/1.1707904.
- (40) Ehrlich, G.; Hudda, F. G. Atomic View of Surface Self-Diffusion: Tungsten on Tungsten. *J. Chem. Phys.* **1966**, *44*, 1039–1049, DOI: 10.1063/1.1726787.
- (41) Schwoebel, R. L. Step Motion on Crystal Surfaces. II. *J. Appl. Phys.* **1969**, *40*, 614–618, DOI: 10.1063/1.1657442.
- (42) Pimpinelli, A.; Elkinani, I.; Karma, A.; Misbah, C.; Villain, J. Step motions on high-temperature vicinal surfaces. *J. Phys.: Condens. Matter* **1994**, *6*, 2661, DOI: 10.1088/0953-8984/6/14/005.
- (43) Paulin, S.; Gillet, F.; Pierre-Louis, O.; Misbah, C. Unstable step meandering with elastic interactions. *Phys. Rev. Lett.* **2001**, *86*, 5538–5541, DOI: 10.1103/PhysRevLett.86.5538.
- (44) ZaLuska-Kotur, M. A.; Krzyzewski, F.; Krukowski, S. Emergence of regular meandered step structure in simulated growth of GaN(0001) surface. *J. Cryst. Growth* **2012**, *343*, 138–144, DOI: <https://doi.org/10.1016/j.jcrysgro.2012.01.033>.
- (45) Thompson, A. P.; Aktulga, H. M.; Berger, R.; Bolintineanu, D. S.; Brown, W. M.; Crozier, P. S.; in 't Veld, P. J.; Kohlmeyer, A.; Moore, S. G.; Nguyen, T. D.; Shan, R.; Stevens, M. J.; Tranchida, J.; Trott, C.; Plimpton, S. J. LAMMPS - a flexible simulation tool for particle-based materials modeling at the atomic, meso, and continuum scales. *Comput. Phys. Commun.* **2022**, *271*, 108171, DOI: 10.1016/j.cpc.2021.108171.
- (46) Zhao, J.; Byggmästar, J.; He, H.; Nordlund, K.; Djurabekova, F.; Hua, M. Complex Ga₂O₃ polymorphs explored by accurate and general-purpose machine-learning interatomic potentials. *npj Comput. Mater.* **2023**, *9*, 159, DOI: 10.1038/s41524-023-01117-1.

- (47) Henkelman, G.; Uberuaga, B. P.; Jónsson, H. A climbing image nudged elastic band method for finding saddle points and minimum energy paths. *J. Chem. Phys.* **2000**, *113*, 9901–9904, DOI: 10.1063/1.1329672.
- (48) Henkelman, G. A.; Jónsson, H. Improved tangent estimate in the nudged elastic band method for finding minimum energy paths and saddle points. *J. Chem. Phys.* **2000**, *113*, 9978–9985, DOI: 10.1063/1.1323224.
- (49) Nosé, S. A molecular dynamics method for simulations in the canonical ensemble. *Mol. Phys.* **1984**, *52*, 255–268, DOI: 10.1080/00268978400101201.
- (50) Hoover, W. G. Canonical dynamics: Equilibrium phase-space distributions. *Phys. Rev. A* **1985**, *31*, 1695–1697, DOI: 10.1103/PhysRevA.31.1695.
- (51) Kresse, G.; Furthmüller, J. Efficiency of ab-initio total energy calculations for metals and semiconductors using a plane-wave basis set. *Comput. Mater. Sci.* **1996**, *6*, 15–50, DOI: 10.1016/0927-0256(96)00008-0.
- (52) Blöchl, P. E. Projector augmented-wave method. *Phys. Rev. B* **1994**, *50*, 17953–17979, DOI: 10.1103/PhysRevB.50.17953.
- (53) Perdew, J. P.; Burke, K.; Ernzerhof, M. Generalized Gradient Approximation Made Simple. *Phys. Rev. Lett.* **1996**, *77*, 3865–3868, DOI: 10.1103/PhysRevLett.77.3865.
- (54) Stukowski, A. Visualization and analysis of atomistic simulation data with OVITO—the Open Visualization Tool. *Modelling Simul. Mater. Sci. Eng.* **2009**, *18*, 015012, DOI: 10.1088/0965-0393/18/1/015012.